NASA-TP-2309

19840024318

Analytical and Experimental Investigation of Stator Endwall Contouring in a Small Axial-Flow Turbine

II — Stage Results

Jeffrey E. Haas
and Robert J. Boyle

NASA

ERRATA

NASA Technical Paper 2309

ANALYTICAL AND EXPERIMENTAL INVESTIGATION OF STATOR ENDWALL
CONTOURING IN A SMALL AXIAL-FLOW TURBINE

Jeffrey E. Haas and Robert J. Boyle
September 1984

Cover, title page, and report documentation page: The following part
title should be added:

II – Stage Results

Analytical and Experimental Investigation of Stator Endwall Contouring in a Small Axial-Flow Turbine

II - Stage Results·

Jeffrey E. Haas
Propulsion Laboratory
USAAVSCOM Research and Technology Laboratories
Lewis Research Center
Cleveland, Ohio

Robert J. Boyle
Lewis Research Center
Cleveland, Ohio

Summary

An experimental and analytical investigation was conducted to determine the effect of stator endwall contouring on turbine stage performance. In this investigation three stator configurations were evaluated using a common rotor. The three stator configurations were a cylindrical endwall design and two contoured endwalls designs, one having an S-shaped outer wall profile and the other having a conical-shaped outer wall profile. Experimental data were obtained over a range of equivalent speeds, total pressure ratios, and rotor tip clearances for each stator-rotor combination. Detailed analytical loss assessments were conducted to aid in the determination of the contouring effect on turbine performance.

The results of the experimental investigation showed that at equivalent design speed and total pressure ratio the total efficiencies were 0.845, 0.851, and 0.853 for the cylindrical endwall, S-shaped endwall contour, and conical-shaped endwall contour configurations, respectively. Agreement was obtained between the computed and measured stage efficiencies for each stator-rotor configuration. The loss assessment showed that reduced stator loss was the major factor in the stage efficiency improvement with contouring. Differences in stator exit flow conditions did not appear to dramatically affect stage efficiency. An evaluation of the rotor tip clearance loss for each stator configuration showed that stator contouring had only a small effect on the tip clearance loss slope.

Introduction

Axial turbines being designed for advanced high-pressure gas generators in the 1- to 5-kg/sec engine airflow size class are characterized by small blade heights (typically less than 2.5 cm), long chord lengths (nominally about 2.5 cm), thickened blade profiles (thickness to chord ratios of about 0.25), and large rotor tip clearance ratios (about 2 percent of the rotor blade height). The efficiency levels associated with these small, low-aspect-ratio turbines are low when compared with large turbines, largely because of Reynolds number effects and size effects such as rotor tip clearance, boundary layer thickness, fillet radius, and surface finish. An important goal of the small turbine research at the NASA Lewis Research Center is to investigate concepts that offer the potential for increasing turbine efficiency. One concept that has this potential is stator endwall contouring. Contouring the stator tip endwall produces more favorable pressure gradients on the vane surfaces and endwalls, thus reducing boundary-layer growth and loss. Contouring can also alter the stator-exit radial loss distribution to improve flow conditions into the rotor.

To provide a better understanding of the loss mechanisms associated with stator contouring, a program was conducted at Lewis to design and evaluate experimentally and analytically two contoured stator endwall designs for a 12.77-cm-tip-diameter axial-flow turbine. The first configuration had an S-shaped outer-wall profile and was designed by using the parametric data reported in reference 1. The second configuration had a conical-convergent outer-wall profile and was designed by simply connecting the stator-inlet and -exit tip diameters with a straight line. A cylindrical endwall stator was also evaluated to provide a reference.

The research program consisted of a stator investigation and a stage investigation. The results of the stator investigation are presented in reference 2 when all three stator configurations were evaluated in a cold-air, full-annular cascade environment. Performance was determined from detailed stator-exit radial and circumferential surveys of flow angle and total pressure. In addition, an analysis method was used to predict the losses for the three stator configurations. The main result from the stator experimental evaluation was that at design stator pressure ratio the reduction in kinetic energy loss coefficient with contouring was 0.005. More importantly, however, contouring enabled the low-momentum fluid at the tip to be contained in the tip region, which would be expected to improve the flow conditions entering following blade rows. Because of differences in the movement of low-momentum fluid, the radial variations in loss for the three stator configurations showed that the two contoured stators had higher loss near the tip and lower loss near the hub than did the cylindrical endwall stator. The main result from the analysis was that the loss attributed to secondary flows was nearly constant for the three stator configurations. The reduction in loss with the two contoured stators was attributed to a reduction in the

boundary-layer growth along the vane surfaces and endwalls.

In the stage investigation, which is presented in this report, all three stator configurations were evaluated using a common rotor to determine the effect of contouring on the overall stage performance. The evaluation consisted of three parts. First, each stator configuration was tested with the common rotor over a range of turbine rotative speeds and pressure ratios at the design rotor tip clearance of 2.4 percent of the rotor blade height. Second, at the design values of equivalent rotative speed, turbine total pressure ratio, and rotor tip clearance, detailed analyses were made for each stator-rotor configuration to determine the causes for the differences in stage efficiency. The analyses were based on the computer programs described in references 3 to 5 plus additional loss correlations described in reference 6 to divide the overall turbine loss for each stator-rotor configuration into individual stator and rotor losses. Finally, for each stator-rotor configuration, experimental data were obtained at two additional values of rotor tip clearance equal to 5.0 and 6.9 percent of the rotor blade height. These data were used to determine if stator endwall contouring caused a change in the rotor tip clearance penalty.

The experimental and analytical performance of each stator-rotor configuration was determined with air at a nominal inlet temperature of 325 K and a nominal inlet pressure of 1.4 bars absolute. These conditions were selected to duplicate the engine Reynolds number and to avoid icing conditions downstream of the rotor. Performance data were taken at total stage pressure ratios from 2.2 to 3.2 and rotative speeds from 60 to 110 percent of equivalent design speed. Rotor exit radial surveys of total pressure, total temperature, and flow angle were made at both equivalent design speed and work and at equivalent design speed and total pressure ratio.

The aerodynamic performance of each stator-rotor configuration is presented in terms of equivalent mass flow, torque, specific work, and efficiency. The results of the analyses are also presented to indicate what caused the differences in stage efficiency among the three stator configurations.

Symbols

c	actual chord, cm
c_x	axial chord, cm
$\bar{e}_r$	rotor kinetic energy loss coefficient, $1 - (W_3^2 / W_{3,id}^2)$
$\bar{e}_s$	stator kinetic energy loss coefficient, $1 - (V_2^2 / V_{2,id}^2)$
$\Delta h'$	specific work, J/g
m	mass flow rate, kg/sec
N	rotative speed, rpm
P	absolute pressure, bars
R_x	rotor reaction, $(P_2 - P_3)/(P_1' - P_3)$
r	radius, cm
s	blade spacing, cm
T	absolute temperature, K
U	blade velocity, m/sec
V	absolute gas velocity, m/sec
ΔV_u	change in absolute tangential velocity, m/sec
W	relative gas velocity, m/sec
α	absolute gas flow angle measured from axial direction, deg
β	relative gas flow angle measured from axial direction, deg
γ	ratio of specific heats
δ	ratio of inlet total pressure to U.S. standard sea-level pressure, P_1/P^*
ϵ	function of δ used in relating parameters to those using air inlet conditions at U.S. standard sea-level conditions, $(0.740/\delta)$ $[(\delta + 1)/2]^{\delta/(\delta-1)}$
η'	efficiency based on total pressure ratio, P_1'/P_3'
η_0'	total efficiency at zero rotor tip clearance
$\Delta\eta_{stage}'$	loss in stage total efficiency
Θ_{cr}	squared ratio of critical velocity at turbine-inlet temperature to critical velocity at U.S. standard sea-level temperature, $(V_{cr}/V_{cr}^*)^2$
μ	viscosity, kg/m sec
Γ	torque, N-m

Subscripts:

cr	condition corresponding to Mach 1
id	ideal
m	mean
R	rotor
S	stator
sur	survey
T	total
0	station at turbine inlet (fig. 1)
1	station at stator inlet (fig. 1)
2	station at stator exit (fig. 1)
3	station at rotor exit (fig. 1)

Figure 1.—Cross-sectional view of turbine.

Turbine Design

In this stage investigation two contoured endwall stator configurations were designed and evaluated. Their performance was compared with that of a reference cylindrical endwall stator configuration. A common rotor was used with all three stator configurations. The cylindrical endwall stator was designed for a single-stage, axial-flow turbine that had a rotor tip diameter of 12.77 cm and a rotor blade height of 1.05 cm. A cross-sectional view of the turbine with the cylindrical endwall stator is shown in figure 1. The instrumentation stations shown in figure 1 are discussed in the **Research Equipment and Procedure** section.

The hot engine and equivalent design conditions are listed in table I. Also tabulated are the conditions at which the turbine was tested. The turbine was designed for an engine flow rate of about 1 kg/sec at an inlet temperature of 1478 K and a pressure of 9.1 bars absolute. The design efficiency was 0.85 at a work factor of 1.67. The turbine design velocity diagrams with the cylindrical endwall stator are shown in figure 2. These diagrams were calculated on a one-dimensional flow basis. The stator-exit flow angle was a constant 74.2° and the rotor-exit relative flow angle was a constant 61.9°.
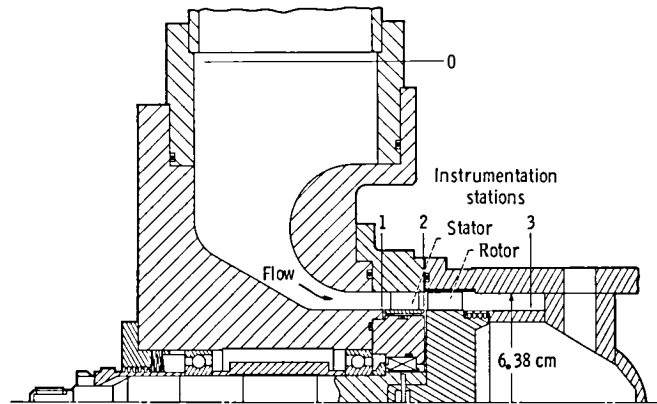
To evaluate the effect of stator endwall contouring, two contoured-endwall stator configurations were designed. For both configurations the same vane untwisted and untapered profile shape as was used for the cylindrical endwall stator was selected. The tip sections were extended to define the outer endwall contour shape. The first contoured-endwall stator configuration (designated contoured stator A) had an S-shaped outer-wall profile and was designed by using the parametric data reported in reference 1. These data indicated that, for an aspect ratio (based on axial chord) of 0.66, an optimum height ratio (inlet height divided by exit height) of about 1.35 should be chosen.

The second contoured-endwall stator configuration (designated contoured stator B) was designed using the same inlet and exit tip diameters as were used for contoured stator A. However, instead of an S-shaped curve along the outer endwall, a straight line was used, thereby providing a conical-convergent configuration.

Station	Hub	Mean	Tip
Radius (cm) at –			
Station 1	5.33	5.86	6.38
Station 2	5.33	5.86	6.38
Station 3	5.33	5.86	6.38
α_2, deg	74.2	74.2	74.2
β_2, deg	56.7	48.2	34.4
α_3, deg	-23.3	-17.5	-11.6
β_3, deg	-61.9	-61.9	-61.9

Station
1, Stator inlet
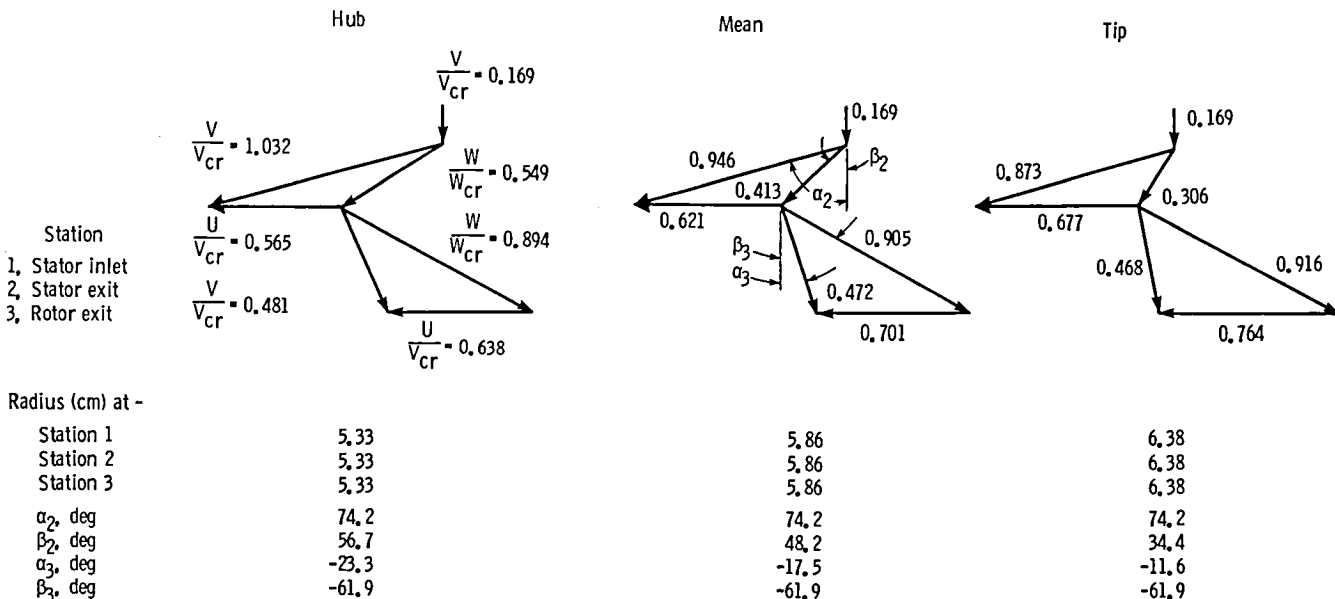2, Stator exit
3, Rotor exit

Figure 2.—Design velocity diagrams (cylindrical endwall stator).

Cross-sectional schematics of the three stator configurations are shown in figure 3. The exit vane height for all three configurations was 1.05 cm. For the two contoured-endwall configurations the inlet vane height was 1.42 cm. Table II lists design parameters for the stator. All three stator configurations had 28 vanes and an aspect ratio of 0.5 based on the exit vane height and the actual chord. The profile and endwall coordinates for the three stator configurations are listed in table III. A photograph of the three stator configurations is shown in figure 4.

The design blade surface velocities for the three stator configurations are shown in figure 5. These were obtained using the MERIDL and TSONIC computer codes (refs. 3 and 4). For TSONIC cases with significant supersonic regions the modifications of reference 7 were used. As a result of high solidity, the surface velocity distributions show the stator to be lightly loaded. Except at the tip, the surface velocities were similar for all three stators. At the hub and mean, the surface velocities were slightly lower for the two contoured stators. This was a result of the increased passage height. When the contour geometry for contoured stator A deflected the tip flow radially inward, the surface velocities decreased. This was followed by a large overshoot in the suction-surface velocity. Since all three stator configurations were lightly loaded, the cross-channel pressure gradients were minimized.

For this research program the same rotor was used with all three stator configurations. The rotor was also untwisted and untapered. Design parameters for the rotor are listed in table IV. There were 30 rotor blades with an aspect ratio of 0.5. Based on the design velocity diagrams in figure 2, the rotor blades had incidence angles from $+16.2°$ to $-6.1°$ and rotor reaction R_x from 0.255 to 0.418 from hub to tip, respectively. The large positive value of rotor hub incidence was attributed to the selection of an untwisted rotor design. An untwisted rotor design was selected because this rotor was used in an earlier research program dealing with the effect of stator and rotor cooling air on turbine performance. An untwisted, untapered cooled rotor was considered easier to fabricate. Rotor coordinates are presented in table V, and a photograph of the rotor is shown in figure 6. The design rotor blade surface velocities are shown in figure 7. These were also calculated by using the MERIDL and TSONIC computer codes. A small amount of diffusion is indicated on the suction surface of all three sections. The rotor is unshrouded and operated in the performance tests with a tip clearance equal to 2.4 percent of the rotor blade height. The rotor tip clearance was obtained by using a recess in the outer casing above the rotor blade tips.

(a) Cylindrical endwall stator.
(b) Contoured stator A.
(c) Contoured stator B.
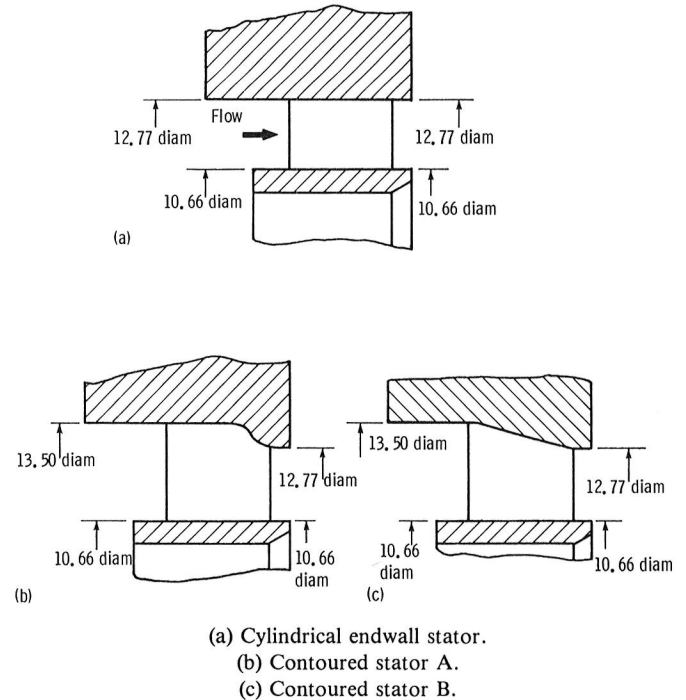
Figure 3.—Schematic cross-sectional view of three stator configurations tested (dimensions in centimeters).
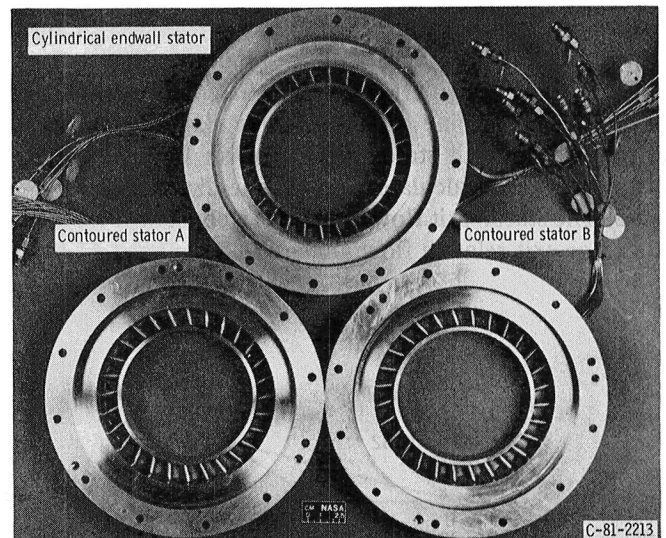
Figure 4.—Stator configurations.

Research Equipment and Procedure

The apparatus used in this investigation consisted of the research turbine, an airbrake dynamometer used to control the speed and absorb and measure the power output of the turbine, an inlet and exhaust piping system including flow controls, and appropriate

(a) Hub.
(b) Mean.
(c) Tip.
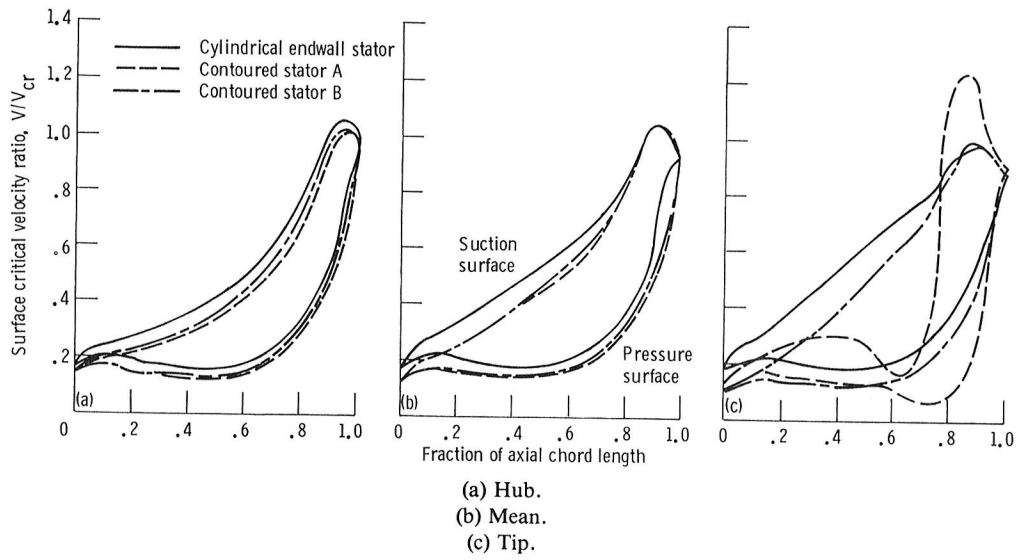
Figure 5.—Design blade surface velocity distributions for three stator configurations.
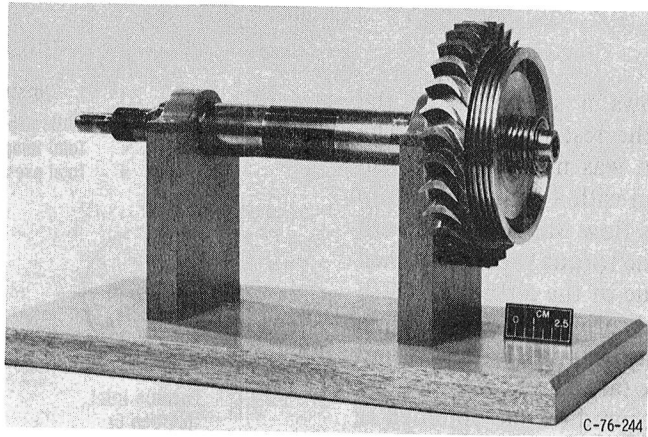
Figure 6.—Rotor assembly.

(a) Hub.
(b) Mean.
(c) Tip.
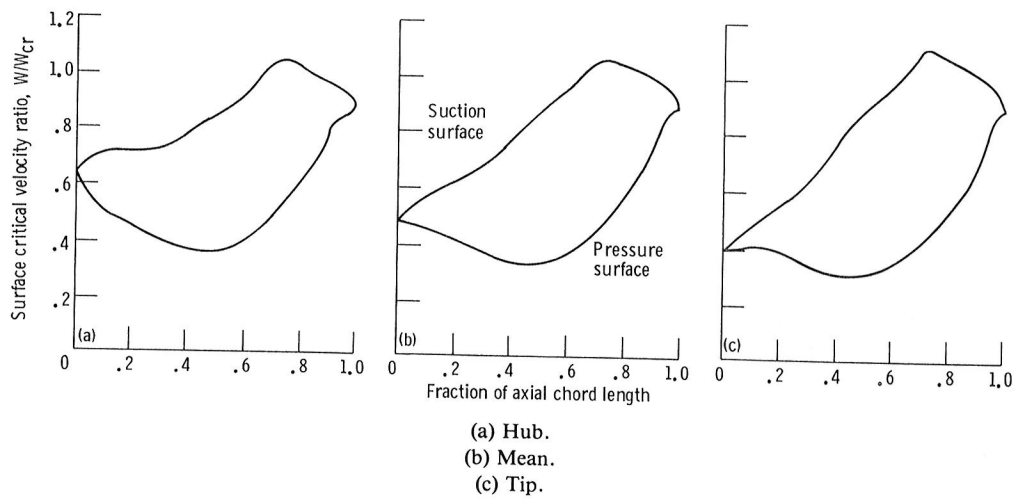
Figure 7.—Design rotor blade velocity distributions.
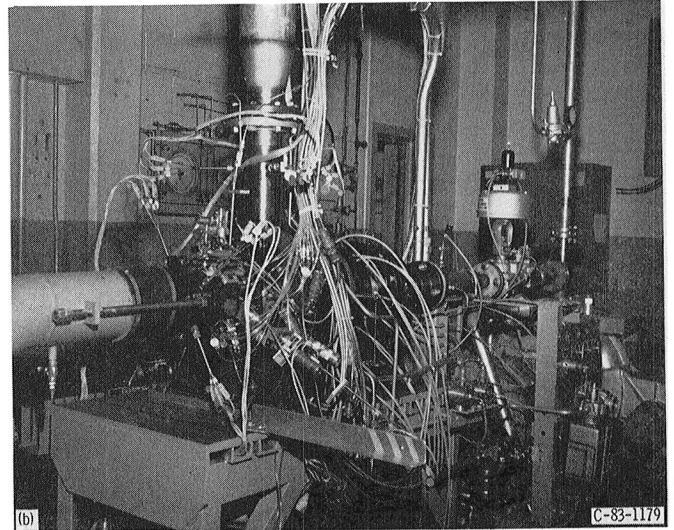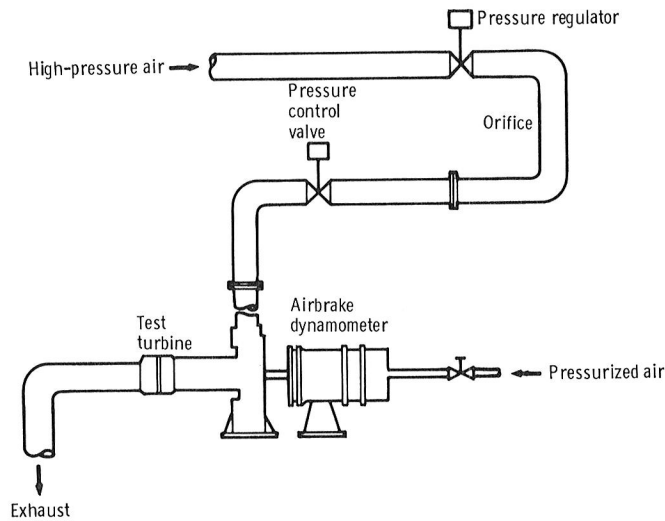
(a) Facility schematic.
(b) Turbine test apparatus.

Figure 8.—Test installation.

instrumentation. Figure 8 shows a schematic of the facility and a photograph of the test installation. The rotational speed of the turbine was measured with an electronic counter in conjunction with a magnetic pickup and a shaft-mounted gear. Mass flow was measured with a calibrated orifice plate. Turbine torque was determined by measuring the reaction torque of the airbrake, which was mounted on air trunnion bearings, and by adding corrections for the turbine bearings and seal losses and the coupling windage loss. These tare losses corresponded to about 2.7 percent of the measured torque obtained at design equivalent speed and pressure ratio. The torque load was measured with a commercial strain-gage load cell.

The turbine instrumentation stations are shown in figure 1. Figure 9 shows the instrumentations at each station. Total temperature was measured at the turbine inlet (station 0) using three thermocouple rakes, each containing three thermocouples at the area center radii of three equal annular areas.

At both the stator inlet (station 1) and the stator exit (station 2) static pressure was measured from eight taps, four on the inner wall and four on the outer wall at different intervals around the circumference.

At the rotor exit (station 3), located about two axial chord lengths downstream of the rotor, static pressure, total pressure, total temperature, and flow angle were measured. The static pressure was measured with eight taps, four each on the inner and outer walls. Three self-aligning probes located around the circumference were used to measure total pressure, total temperature, and flow angle. The location of station 3 was selected so that the rotor-exit instrumentation would be located where there would be no rotor wake effects.

Instrumentation
• Static pressure
× Total temperature
⊖ Total pressure and flow angle

Turbine inlet (station 0)

Stator inlet (station 1)

Stator exit (station 2)

Rotor exit (station 3)
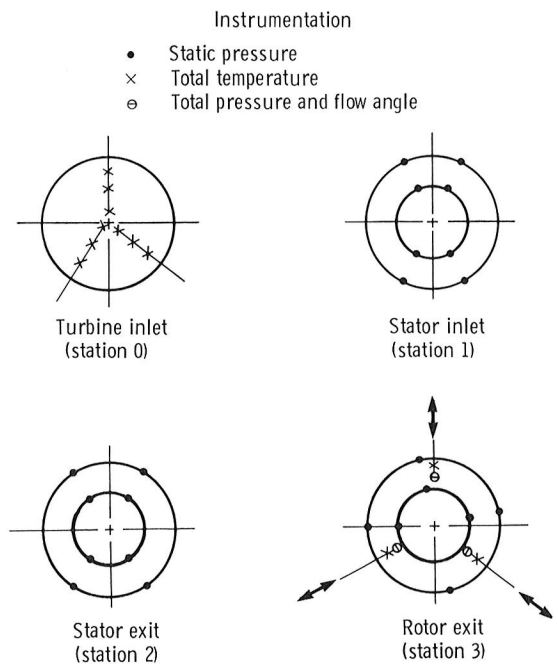
Figure 9.—Flow path instrumentation, viewed looking downstream.

The stage experimental program consisted of two parts. First, the three stator configurations were each tested with the common rotor over a range of turbine rotative speeds from 60 to 110 percent of equivalent design speed and a range of total pressure ratios from 2.2 to 3.2. The tests were conducted at the hot-engine Reynolds number listed in table I and with the design rotor tip clearance of 2.4 percent of the rotor blade height. In the second part of the experimental program, data were obtained for each stator-rotor configuration at two additional values of rotor tip clearance equal to 5.0

6

and 6.9 percent of the rotor blade height. At each clearance, data were obtained for total pressure ratios from 2.2 to 3.2 at design equivalent speed. The rotor tip clearance was changed by replacing a ring in the casing over the rotor blade tips. The inner diameter of the two additional rings was machined to provide the different tip clearances. The rotor tip diameter remained unchanged throughout the test program.

For both parts of the experimental program a rotor-exit survey was first conducted at equivalent design values of speed and work. Mass-averaged values of flow angle, total temperature, and total pressure were obtained for each of the three circumferential survey locations at station 3. These mass-average values were averaged arithmetically to obtain overall values. The survey probes were then positioned with one each near the tip, near midspan, and near the hub so that the average flow angle from these three positions would correspond closely to the overall mass-averaged value obtained from the survey. Performance data were then obtained at other operating conditions. To aid in subsequent data analysis, a rotor-exit survey was also conducted for each stator-rotor configuration at equivalent design values of speed and total pressure ratio.

The stage evaluation was conducted in air at nominal inlet conditions of 325 K and a nominal turbine-inlet pressure of 1.4 bars absolute. The turbine was rated on the basis of total efficiency. The actual work was calculated from torque, speed, and mass flow measurements. The ideal work was based on the stator-inlet to rotor-exit total pressure ratio. The stator-inlet (station 1) and rotor-exit (station 3) total pressures were calculated from mass flow, static pressure, total temperature, and flow angle. For the calculation of stator-inlet total pressure, the flow angle was assumed to be zero.

Analysis Method

To obtain a more detailed understanding of the reasons for the efficiency differences among the three stator-rotor configurations, detailed loss analyses were conducted at design equivalent speed and pressure ratio. A detailed explanation of the analysis method is given in reference 6. The analysis method uses the MERIDL and TSONIC computer codes to compute the blade surface and endwall velocities in the stator and rotor. The BLAYER computer code is then used to calculate stator and rotor boundary-layer displacement and momentum thicknesses, which are then used to calculate profile friction losses (including the mixing loss) and endwall friction losses. Additional published correlations discussed in reference 6 are used to calculate losses due to incidence, secondary flow, rotor tip clearance, disk windage, and exhaust duct friction between the rotor trailing edge and station 3. Losses are calculated as kinetic energy loss coefficients for the stator and rotor. For each blade row the overall kinetic energy loss coefficient is converted into a stage efficiency loss using the following equations from reference 6:

$$\eta' = \frac{\left(\dfrac{P_1'}{P_3'}\right)^{\frac{\gamma-1}{\gamma}} - \left[1 - \bar{e}_{T,R} + \bar{e}_{T,R}\left(\dfrac{P_2''}{P_3}\right)^{\frac{\gamma-1}{\gamma}}\right]\left[1 - \bar{e}_{T,S} + \bar{e}_{T,S}\left(\dfrac{P_1'}{P_2}\right)^{\frac{\gamma-1}{\gamma}}\right]}{\left(\dfrac{P_1'}{P_3'}\right)^{\frac{\gamma-1}{\gamma}} - 1} \quad (1)$$

$$\Delta\eta'_{stage}(stator) = 1 - \frac{\left(\dfrac{P_1'}{P_3'}\right)^{\frac{\gamma-1}{\gamma}} - \left[1 - \bar{e}_{T,S} + \bar{e}_{T,S}\left(\dfrac{P_1'}{P_2}\right)^{\frac{\gamma-1}{\gamma}}\right]}{\left(\dfrac{P_1'}{P_3'}\right)^{\frac{\gamma-1}{\gamma}} - 1} \quad (2)$$

for $\bar{e}_{T,R} = 0$, and

$$\Delta\eta'_{stage}(rotor) = (1 - \eta') - \Delta\eta'_{stage}(stator) \quad (3)$$

The stage efficiency losses for the stator and rotor were added to that for the exhaust duct to calculate an overall stage efficiency. The results of the analyses are presented in the Results and Discussion section.

Results and Discussion

The results of this investigation are presented in three sections. The first section presents the measured

7

performance of the three stator-rotor configurations. Results are presented in terms of mass flow, torque, specific work, total efficiency, rotor exit surveys, and experimental velocity diagrams. The second section discusses the results of the analyses that were conducted to determine the causes for the stage efficiency differences among the three stator-rotor configurations. The third section discusses the results of varying the rotor tip clearance for each of the three stator-rotor configurations.

Experimental Performance

Mass flow.—The variation in equivalent mass flow with stage total pressure ratio and rotor speed for the three stator-rotor configurations is shown in figure 10. The design value given in the figure is the design flow rate for the cylindrical endwall stator. The data indicate that there was a choked stator condition for the cylindrical endwall stator, whereas both contoured stator configurations showed a slight rotor speed effect. At design equivalent speed and total pressure ratio, the equivalent mass flow rates were 0.268, 0.284, and 0.272 kg/sec for the cylindrical endwall, contoured stator A, and contoured stator B configurations, respectively. The mass flow rate for the cylindrical endwall stator was 8.9 percent larger than design. This higher than design flow was attributed primarily to two factors. Stator throat measurements indicated that the cylindrical endwall stator had a throat area 7.2 percent larger than that required to pass design flow. In addition, at the design

equivalent speed and stage pressure ratio of 2.77, the stator pressure ratio P_1'/P_{2m} was 2.01 compared to a design value of 1.8. The design stator pressure ratio occurred at a stage total pressure ratio of about 2.2, where the flow rate was about 3.4 percent less than at design stage pressure ratio.

Stator throat measurements for the contoured stator A and contoured stator B indicated throat areas that were 9.6 and 4.3 percent larger than the cylindrical endwall stator, respectively. The stator pressure ratios for the contoured stator A and contoured stator B were 1.82 and 1.91, respectively, at design equivalent speed and stage pressure ratio of 2.77. Rotor throat measurements indicated that the rotor throat area was 9.0 percent larger than that required to pass design flow. Because of the differences in the stator-rotor throat area ratios among the three stator configurations, there were different stator pressure ratios and different levels of rotor reaction at the design equivalent speed and pressure ratio condition. The effect on turbine performance of these different stator pressure ratios will be discussed later.

Torque.—The variation of equivalent torque with stage total pressure ratio and rotor speed for the three stator-rotor configurations in shown in figure 11. The design value given in the figure is the design equivalent torque for the cylindrical endwall stator. At equivalent design speed and total pressure ratio the measured torque for the cylindrical endwall stator was 5.02 N-m. This was 8.2 percent higher than the design torque, due primarily to the mass flow rate being 8.9 percent larger than design. For the contoured stators A and B, the measured torques were 5.36 and 5.14 N-m, respectively, at design equivalent speed and pressure ratio. These measured torque values were 6.8 and 2.4 percent higher than the torque for the cylindrical endwall stator and were consistent with the higher mass flows for the two contoured stator configurations.

Specific work.—The variation in specific work with stage total pressure ratio and rotor speed for the three stator-rotor configurations is shown in figure 12. At design equivalent speed and pressure ratio the specific work was 61.7, 62.2, and 62.3 J/g for the cylindrical endwall, contoured stator A, and contoured stator B configurations, respectively. The design equivalent specific work was 62.1 J/g.

Total efficiency.—The variation in total efficiency with stage total pressure ratio and rotor speed for the three stator-rotor configurations is shown in figure 13. The three configurations attained stage efficiencies from 0.71 to 0.87 over the range of test conditions. At design equivalent speed and pressure ratio, the total efficiencies were 0.845, 0.851, and 0.853 for the cylindrical endwall, contoured stator A, and contoured stator B configurations, respectively. A discussion of the reasons for the differences in the stage efficiency among the three stator configurations will be presented later in the report.

(a) Cylindrical endwall stator.
(b) Contoured stator A.
(c) Contoured stator B.
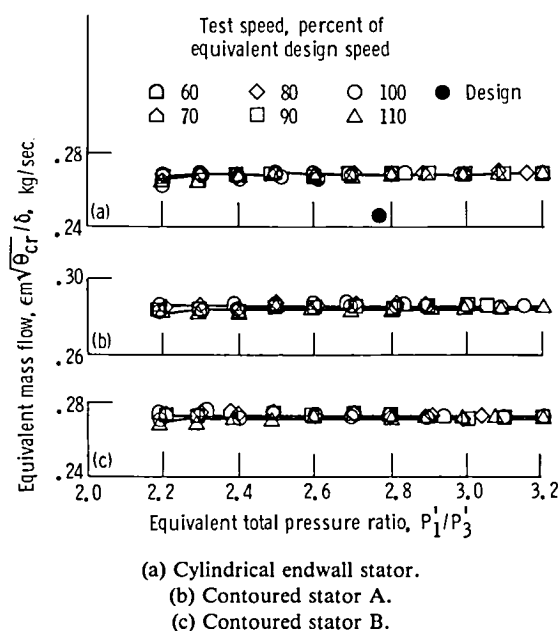
Figure 10.—Variation of equivalent mass flow with total pressure ratio and speed for three stator configurations.

8

(a) Cylindrical endwall stator.
(b) Contoured stator A.
(c) Contoured stator B.
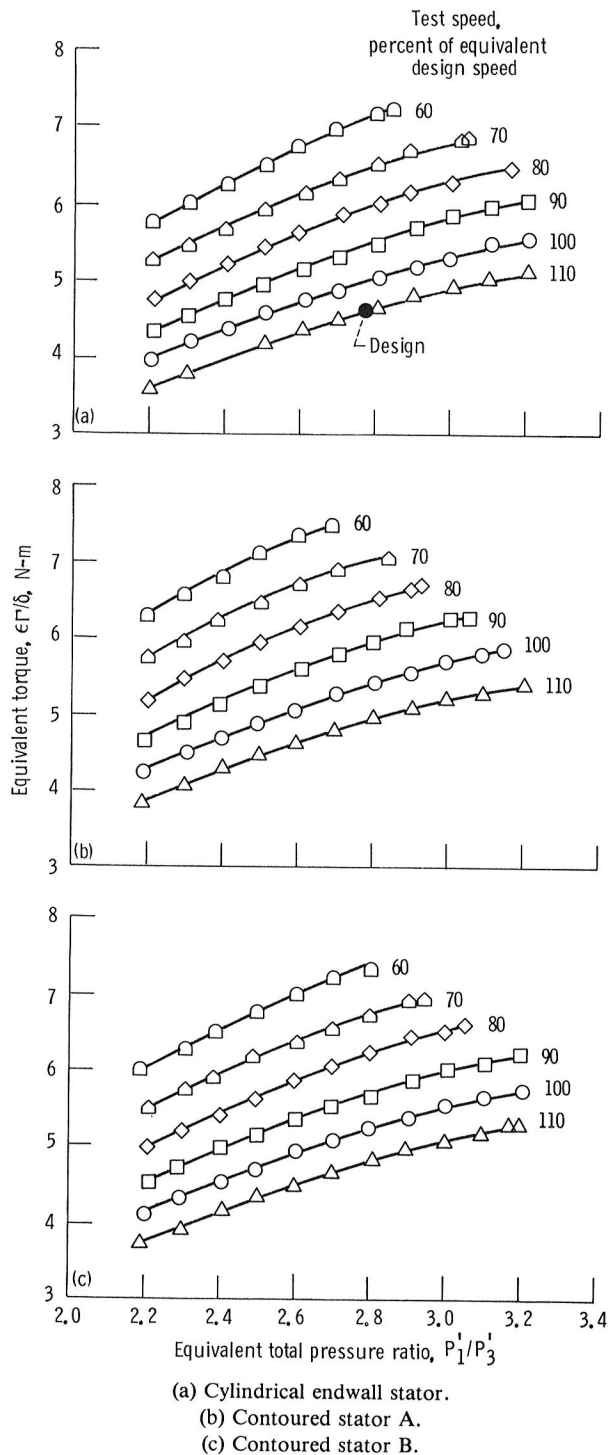
Figure 11.—Variation of torque with total pressure ratio and speed for three stator configurations.

(a) Cylindrical endwall stator.
(b) Contoured stator A.
(c) Contoured stator B.

Figure 12.—Variation of specific work with total pressure ratio and speed for three stator configurations.

Rotor-exit survey.—The results of the radial surveys at station 3 of total temperature, total pressure, and flow angle are shown in figure 14(a), (b), and (c) for each stator-rotor configuration. The measurements were taken with the turbine operating at equivalent design speed and total pressure ratio. The data shown are the averages of the measurements of the three combination probes. With these measurements the radial variation in stage efficiency was calculated and is presented in figure 14(d). The dashed curves in the figure represent the calculated design radial variations based on the design velocity diagrams for the cylindrical endwall stator.

The temperature measurements (fig. 14(a)) indicated nearly constant work for all three stator-rotor configurations. The contoured stator B had the highest work (lowest temperature ratio), whereas the cylindrical endwall stator had the lowest work. This was consistent with the variation in total efficiency (fig. 13). The upswing in temperature near the tip wall was attributed to conduction effects.

The total pressure measurements (fig. 14(b)) indicated variations that were slightly lower than design near the hub and were slightly higher than design near the tip. The decrease in total pressure at the tip was attributed to tip clearance effects. There was only a 1.5-percent variation

Test speed,
percent of equivalent
design speed

(a) Cylindrical endwall stator.
(b) Contoured stator A.
(c) Contoured stator B.
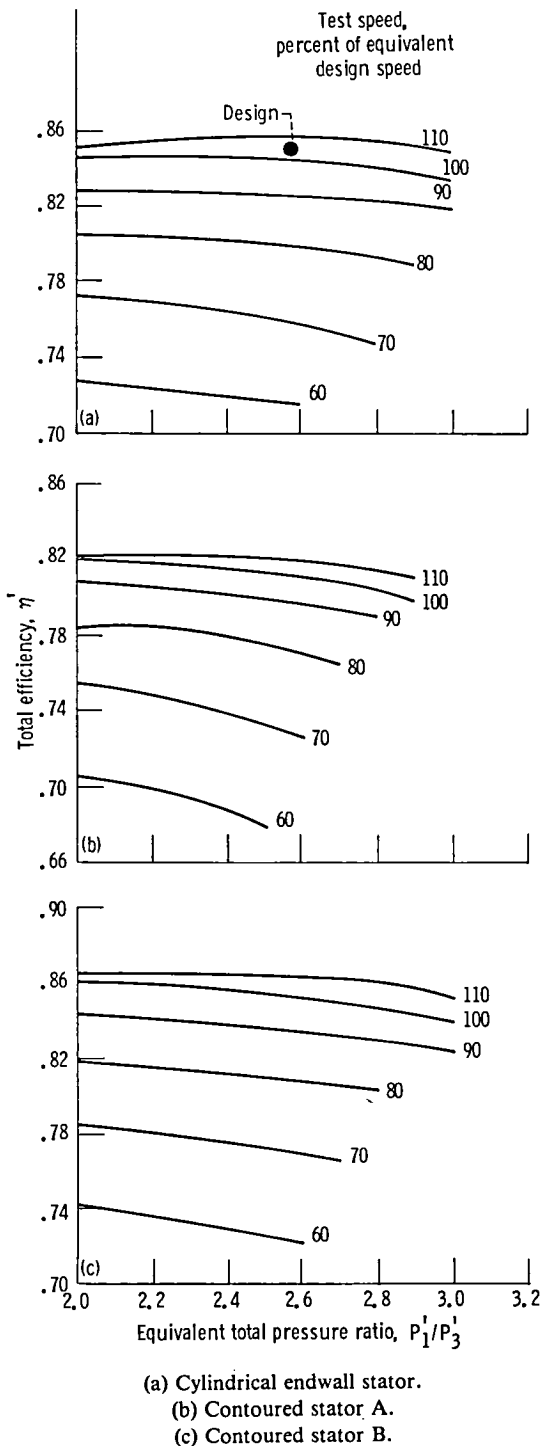
Figure 13.—Variation of total efficiency with total pressure ratio and speed for three stator configurations.

(a) Temperature ratio.
(b) Total pressure ratio.
(c) Flow angle.
(d) Total efficiency.

Figure 14.—Rotor-exit survey at design pressure ratio and speed.

in the mass-averaged total pressure ratios among the three stator-rotor configurations.

The flow angle variations (fig. 14(c)) show that the contoured stator A had the highest negative level of flow angle, whereas the cylindrical endwall stator had the lowest. A negative flow angle indicates a positive contribution to work. The measured flow angles were within ±10° of the design variation. In the stator-exit survey tests (ref. 2) both contoured stator configurations showed a higher stator-exit flow angle near the tip, whereas the cylindrical endwall stator had higher turning from the hub to about 50 percent of the stator-exit blade height. The rotor exit flow angle measurements did not show these trends.

The radial variations in total efficiency (fig. 14(d)) show that both contoured stators had similar trends. The contoured stators also had efficiency levels higher than that for the cylindrical endwall stator over almost all of the blade span. These trends were different than those shown in the stator-exit survey tests (ref. 2). The radial variations in the stator after-mixed kinetic energy loss coefficient for the three stator configurations indicated that the cylindrical endwall stator had lower loss near the tip and higher loss near the hub than did the two contoured configurations. This difference in trends

between the stator and stage tests was attributed to the mixing effects that occur in the rotor.

Mass-averaged values of total efficiency were calculated from figure 14(d) and were compared to the efficiencies shown in figure 13 that were computed from torque, speed, and mass flow data. The mass-averaged efficiencies for the two contoured stator configurations were about one point lower than their respective torque-derived efficiencies, and the mass-averaged efficiency for the cylindrical endwall stator was about two points lower.

Experimental velocity diagrams.—Experimental velocity diagrams were calculated for each of the three stator-rotor configuration at equivalent design speed and pressure ratio using the rotor-exit survey results discussed in figure 14 along with the stator survey results discussed in reference 2. Velocity diagrams were computed at the 5-, 50-, and 95-percent span positions using the measured rotor-exit total temperatures, total pressures, and flow angles and the measured stator-exit flow angles and stator efficiencies.

A comparison of the experimental velocity diagrams for the cylindrical endwall stator (fig. 15(a)) with the design velocity diagrams (fig. 2) shows reasonable agreement. Based on the velocity diagrams, the experimental hub-to-tip variation in rotor reaction R_x was calculated to be 0.214 to 0.426 and the rotor incidence angle hub-to-tip variation was calculated to be $+20.0°$ to $-7.1°$. These compare correspondingly to the design radial variations of 0.255 to 0.418 and $+16.2°$ to $-6.1°$.

A comparison of the experimental velocity diagrams for the cylindrical endwall stator with those for the two contoured stators shows that the contoured stator configurations had generally lower stator velocities and higher rotor velocities (resulting in higher rotor reaction) and lower rotor inlet relative flow angles (resulting in more negative incidence angles). The mass-averaged values of rotor reactions R_x were 0.380 and 0.338 for the contoured stator A and B configurations, respectively, compared to 0.325 for the cylindrical endwall stator. The higher levels of rotor reaction for the two contoured stators were attributed primarily to the larger stator-rotor throat area ratios. For the contoured stators A and B, respectively, the hub-to-tip variations in rotor incidence angle were 9.6° to $-1.1°$ and 10.3° to 1.2. Thus, the level and range of rotor incidence were lower for both contoured stators compared to the cylindrical endwall stator. The lower levels of rotor incidence were also attributed to the larger stator-rotor throat area ratios. The larger stator-rotor throat area ratios caused lower stator pressure ratios for both contoured stator configurations compared to the cylindrical endwall stator at the design equivalent speed and stage pressure ratio condition. Lower stator pressure ratios caused lower

stator-exit absolute velocities and lower rotor inlet relative velocities and relative flow angles. The effect of the lower rotor incidence angles on performance is discussed in the next section.

Analytical Results

The analytical results are presented in two sections. The first section compares velocity diagrams calculated from the MERIDL program for all three stator-rotor configurations at design equivalent speed and total pressure ratio with the experimental velocity diagrams discussed in figure 15. The second section discusses the loss assessments that were made at design equivalent speed and total pressure ratio using the procedure outlined in the **Analysis Method** section.

Calculated velocity diagrams.—The basis for the detailed loss assessments are the stator and rotor velocities and flow angles calculated from the MERIDL program. A comparison of velocity diagrams computed from the MERIDL program at design equivalent speed and total pressure ratio with the experimental velocity diagrams presented in figure 15 provides a partial assessment of how well the analysis method modeled the experiment. Since there were no static pressure taps on the stator or rotor blading from which experimental blade loadings could be computed, only a comparison of computed and experimental velocities and flow angles at the stator and rotor exits could be made.

A comparison of figures 15 and 16 shows agreement between the analytical and experimental velocities and flow angles at the mean section of all three stator-rotor configurations. At the hub and tip sections bigger differences exist between the analytical and experimental results. This is not unexpected since MERIDL is an inviscid program which calculates flow conditions along a hub-to-shroud midchannel stream surface. Factors such as endwall boundary layer skewing and three-dimensional tip clearance effects are not accounted for.

Loss assessments.—A detailed loss assessment was conducted for each of the three stator-rotor configurations at design equivalent speed and stage total pressure ratio using the procedure discussed in the **Analysis Method** section. For each stator-rotor configuration the analysis was conducted using the experimental values of turbine-inlet temperature and pressure, mass flow, stator-inlet boundary-layer thicknesses on each wall (obtained from ref. 2) and the stator pressure ratio. As was discussed earlier, there were different mass flows and stator pressure ratios for each stator-rotor configurations at the equivalent design speed and total pressure ratio condition.

5-Percent span

$\dfrac{V}{V_{cr}} = 1.059$ $\dfrac{V}{V_{cr}} = 0.184$

$\dfrac{W}{W_{cr}} = 0.566$

Station
1, Stator inlet $\dfrac{U}{V_{cr}} = 0.571$ $\dfrac{W}{W_{cr}} = 0.863$
2, Stator exit
3, Rotor exit $\dfrac{V}{V_{cr}} = 0.409$ $\dfrac{U}{V_{cr}} = 0.649$

Mean

0.978   0.184 β_2 α_2

0.621 β_3 α_3 0.459   0.928

0.563   0.699

95-Percent span

0.887   0.184   0.340

0.670   0.942

0.516   0.754

(a)

	5-Percent span	Mean	95-Percent span
α_2, deg	75.9	72.5	72.5
β_2, deg	60.5	46.7	33.4
α_3, deg	-26.5	-10.7	-11.8
β_3, deg	-66.2	-55.5	-59.6

0.140   0.999   0.525   0.571   0.927   0.482   0.647

0.940   0.140   0.449   0.621   0.605   0.984   0.699

0.793   0.140   0.184   0.670   1.023   0.595   0.754

(b)

	5-Percent span	Mean	95-Percent span
α_2, deg	71.6	69.2	80.2
β_2, deg	50.1	37.7	39.4
α_3, deg	-30.2	-15.8	-17.5
β_3, deg	-64.9	-56.0	-58.7

0.134   1.003   0.528   0.571   0.910   0.468   0.646

0.982   0.134   0.475   0.621   0.561   0.933   0.700

0.866   0.134   0.277   0.670   0.971   0.550   0.756

(c)

	5-Percent span	Mean	95-Percent span
α_2, deg	71.9	71.0	77.0
β_2, deg	50.8	43.9	41.7
α_3, deg	-28.5	-11.8	-13.0
β_3, deg	-64.7	-56.0	-58.6

(a) Cylindrical endwall stator.
(b) Contoured stator A.
(c) Contoured stator B.

Figure 15.—Velocity diagrams calculated from experimental data.

The computed losses are shown in table VI. In order to compare the computed stator losses with the measured losses from reference 2, additional analyses were made using the stator-inlet conditions from the stator survey tests. This was necessary since the stator tests were conducted at a Reynolds number R_x of about 4.1×10^5 compared to the stage test value of 3.1×10^5. The results of the additional analyses are shown in parentheses in table VI. Excellent agreement was obtained between the total computed and measured stator kinetic energy loss coefficients for all three stator configurations. When the stator losses were computed for the stage test inlet conditions, the total kinetic energy loss coefficients increased by 0.001 to 0.004 due to the Reynolds number

Hub   Mean   Tip

$\frac{V}{V_{cr}} = 0.183$ 0.183   0.183

$\frac{V}{V_{cr}} = 1.102$ 1.013   0.936
                                       α2   0.368
                                       β2
$\frac{W}{W_{cr}} = 0.647$ 0.621   0.493   0.677

Station
1, Stator inlet $\frac{U}{V_{cr}} = 0.565$ β3   0.539   0.909
2, Stator exit   α3   0.884
3, Rotor exit $\frac{W}{W_{cr}} = 0.859$ 0.496   0.706   0.761

$\frac{V}{V_{cr}} = 0.486$ $\frac{U}{V_{cr}} = 0.639$

	Hub	Mean	Tip
α2, deg	70.4	72.6	73.9
β2, deg	51.9	48.7	40.5
α3, deg	-15.3	-9.5	-3.1
β3, deg	-58.6	-58.5	-55.7

(a)

0.137   0.137   0.135
1.023   0.585   0.951   0.446   0.874   0.301
0.565   0.616   0.677
           0.962   0.972   0.986
0.549   0.567   0.575
     0.640   0.706   0.764

	Hub	Mean	Tip
α2, deg	67.4	71.2	74.8
β2, deg	43.9	42.8	36.0
α3, deg	-27.8	-17.5	-12.1
β3, deg	-61.5	-58.3	-57.5

(b)

0.135   0.134   0.134
1.061   0.627   0.988   0.480   0.907   0.303
0.565   0.615   0.677
           0.920   0.929   0.938
0.516   0.524   0.549
     0.640   0.707   0.763

	Hub	Mean	Tip
α2, deg	67.0	71.6	77.8
β2, deg	44.9	45.8	47.4
α3, deg	-23.8	-14.7	-6.6
β3, deg	-60.9	-58.9	-56.6

(c)

(a) Cylindrical endwall stator.
(b) Contoured stator A.
(c) Contoured stator B.

Figure 16.—Calculated velocity diagrams based on MERIDL output.

effect. These total stator kinetic energy loss coefficients were converted using equation (2) into stage efficiency losses. The different stator pressure ratios caused stage efficiency losses for the two contoured stators that were between 0.005 and 0.009 lower than the losses for the cylindrical endwall stator. The reduction in total stator loss for the two contoured stators was due to a reduction in the profile and endwall friction losses. Stator secondary flow loss was nearly constant among the three stator configurations.

A comparison of the rotor losses shows a significant reduction in the total rotor kinetic energy loss coefficients for both contoured stator configurations. About half of the overall rotor loss was due to rotor tip clearance loss. Most of the loss reduction for the two contoured stator configurations was due to reduced rotor incidence loss.

13

The lower rotor incidence angles for the contoured stator configurations were discussed in the *Experimental velocity diagram* section. Because of the effect of higher rotor pressure ratio, when the total rotor kinetic energy loss coefficients were converted into stage efficiency losses, the losses were about 0.004 lower for the two contoured stator configurations.

The computed stage efficiencies were 0.847, 0.859, and 0.857 for the cylindrical endwall, contoured stator A, and contoured stator B configurations, respectively. These computed values agreed well with the corresponding measured values. The computed efficiencies were higher than their respective measured values by between 0.002 and 0.008. The computed stage efficiencies showed a slightly higher efficiency for contoured stator A compared to contoured stator B, whereas the experimental data showed slightly higher stage efficiency for contoured stator B.

Based on the losses tabulated in table VI, it was determined that the improvement in stage efficiency for the contoured stator A was due primarily to reduced stator loss, whereas for contoured stator B the stage efficiency improvement was equally split between reduced stator loss and reduced rotor loss. Because of the higher rotor pressure ratios, the lower rotor incidence loss for the contoured stator configurations had a small impact on the turbine stage efficiency.

As was noted in the **Turbine Design** section, the two contoured stator configurations were designed by extending the tip sections to define the tip endwall contour shapes. This design approach resulted in different stator throat areas, which caused the rotor incidence angle and rotor reaction differences to occur. An alternate design approach would have been to maintain the same stator throat areas by reducing the throat areas of the two contoured stators. This could have been accomplished by restaggering the stator vanes. Because of the high vane exit blade angle (72.4°), the contoured stator A would have been restaggered by only 1.6° and the contoured stator B by only 0.7° to match the cylindrical endwall stator throat area. This alternate design approach would have been perhaps more practical from an overall engine cycle standpoint, since turbine mass flow would have remained the same.

In order to isolate the effect of stator endwall contouring on stage performance a second loss assessment was made. For this assessment the stator vane shape was plotted and then rotated by 1.6° and 0.7°, respectively, to cause reduced stator throat areas for the contoured stator A and B configurations. New vane coordinates were generated and input into the MERIDL program. The loss analysis was then repeated for both contoured stator configurations.

The results of this second loss assessment are tabulated in table VII. Unlike the initial loss assessment (table VI) where different mass flows and stator pressure ratios were used for each of the three stator-rotor configurations, the cylindrical endwall stator mass flow and stator pressure ratio were used as boundary conditions for both contoured stator configurations for the results shown in table VII. This approach seemed reasonable, since for this second loss assessment the two contoured stator configurations would have had the same stator-rotor throat area ratio as for the cylindrical endwall stator configuration.

Table VII shows that the computed stage efficiencies for the two contoured stator configurations were 0.004 less than those calculated initially (table VI). The total stator kinetic loss coefficients for the two contoured stators were 0.002 less than those in table VI. However, the higher stator pressure ratios for the two contoured stators caused the stage efficiency losses to be higher than those shown in table VI by between 0.001 and 0.004. The total rotor kinetic energy loss coefficients for the three configurations were nearly the same. In fact, there were only small differences in each of the individual rotor losses. Even the rotor incidence loss was nearly the same because of higher rotor inlet relative flow velocities and angles caused by the higher stator pressure ratio. The nearly constant total rotor loss indicates that even though the three stator configurations had different stator exit radial angular momentum distributions the rotor performance was essentially independent of these differences. The results tabulated in table VII show that the increases in stage efficiency that occurred with both contoured stator configurations were due more to reduced stator losses than to reduced rotor losses.

Effect of Rotor Tip Clearance

An additional part of the experimental investigation was to evaluate the effect of rotor tip clearance on the performance of the three stator-rotor configurations. In small turbines the tip clearance loss is a significant portion of the overall turbine loss. Because contoured stators are widely used in current turbine designs and because all the published tip clearance loss data were obtained from turbine designs with cylindrical endwall stators, additional testing was conducted to determine whether or not stator contouring had an effect on the rotor tip clearance loss. Because of the different stator-exit radial loss distributions that were noted in the stator investigation (ref. 2), the thought existed that stator contouring could influence the rotor tip clearance loss.

For this tip clearance investigation, each stator-rotor configuration was tested at the design rotor tip clearance of 2.4 percent of the rotor blade height and at two additional values of rotor tip clearance equal to 5.0 and 6.9 percent of the rotor blade height. At each clearance, data were obtained over a range of total pressure ratios at design equivalent speed. The results of the investigation
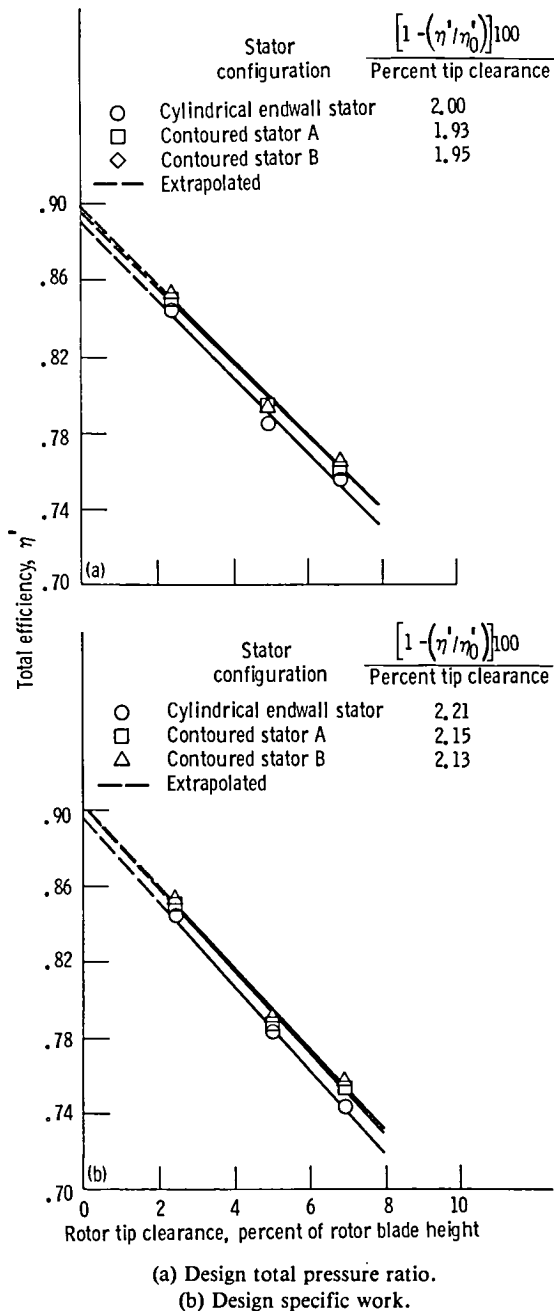
Stator configuration	$\dfrac{[1-(\eta'/\eta_0')]100}{\text{Percent tip clearance}}$
O Cylindrical endwall stator	2.00
□ Contoured stator A	1.93
◇ Contoured stator B	1.95
—— Extrapolated	

Stator configuration	$\dfrac{[1-(\eta'/\eta_0')]100}{\text{Percent tip clearance}}$
O Cylindrical endwall stator	2.21
□ Contoured stator A	2.15
△ Contoured stator B	2.13
—— Extrapolated	

(a) Design total pressure ratio.
(b) Design specific work.

Figure 17.—Variation of total efficiency with rotor tip clearance for three stator configurations.

are shown in figure 17. Turbine efficiency is plotted against rotor tip clearance. In figure 17(a) the efficiency data for each stator-rotor configuration at the three rotor tip clearances is for the design equivalent speed and total pressure ratio condition. In figure 17(b) the efficiency data are for the design equivalent speed and specific work condition. Both figures show separate levels of efficiency for each stator configuration but essentially the same tip clearance loss slope, expressed as a decrease in total efficiency per percent increase in rotor tip clearance. For the design total pressure ratio condition, the tip clearance

loss slope varied from 1.93 to 2.00, whereas for the design specific work condition, the loss slope varied from 2.13 to 2.21. The higher loss slope for the design specific work condition was attributed to the effect of operating at much higher stage pressure ratios at the higher rotor tip clearance values. The results shown in figure 17 indicate that stator contouring had only a small effect on the rotor tip clearance loss slope.

Concluding Remarks

Based on the results obtained for both this investigation and the previous stator survey investigation, it can be concluded that stator contouring does improve turbine efficiency. This investigation showed that the improvement in stage efficiency was due largely to reduced stator loss, particularly reduced stator blade and endwall friction losses. Even though stator contouring caused significant differences in secondary flow movement, the different stator exit radial loss distributions did not appear to affect rotor performance. The use of a conical-convergent stator was shown to give the same level of efficiency improvement as use of a S-contour stator. In addition, the analysis provided valuable insight into the reasons for the stage efficiency improvement due to contouring. The agreement between the computed and measured stage efficiencies was considered sufficiently accurate.

In this investigation the amount of efficiency improvement was about 0.007. The turbine stator blading used had high solidity stator blading. High solidity blading results in light loading and well accelerated flow. The effects of contouring may be larger in low solidity blading because the blading is more heavily loaded, and the unloading that takes place with contouring would be more pronounced. A detailed experimental and analytical study of the effect of stator contouring on the performance of a low stator solidity turbine design would be the next area to investigate.

Summary of Results

An experimental and analytical investigation was conducted to determine the effect of stator endwall contouring on turbine stage performance. In this investigation three stator configurations were evaluated using a common rotor. The three stator configurations were a cylindrical endwall design and two contoured endwall designs, one having an S-shaped outer wall profile and the other having a conical-shaped outer wall profile.

Experimental data were obtained over a range of equivalent speeds, total pressure ratios, and rotor tip clearances for each stator-rotor combination. Detailed

15

analytical loss assessments were conducted to aid in the determination of the contouring effect on turbine performance. The results of the investigation may be summarized as follows:

(1) At equivalent design speed and total pressure ratio, the experimental total efficiencies were 0.845, 0.851, and 0.853 for the cylindrical endwall, S-shaped endwall contour, and conical-shaped endwall contour configurations, respectively.

(2) Agreement was obtained between the computed and measured stage efficiencies for each stator-rotor configuration. The loss assessments showed that reduced stator loss was the major factor in the stage efficiency improvement with contouring. Differences in stator-exit flow conditions among the stator configurations did not appear to dramatically affect turbine stage efficiency.

(3) An evaluation of rotor tip clearance loss for each stator configuration showed that stator contouring had only a small effect on the tip clearance loss slope.

Lewis Research Center
National Aeronautics and Space Administration
Cleveland, Ohio

References

1. Deich, M.E.; et al.: Method of Increasing the Efficiency of Turbine Stages and Short Blades. Translation No. 2816, Associated Electrical Industries Ltd., Manchester, England, 1960.
2. Haas, J. E.: Analytical and Experimental Investigation of Stator Endwall Contouring in a Small Axial-Flow Turbine. I: Stator Performance. NASA TP-2023, 1982.
3. Katsanis, T.; and McNally, W. D.: Revised FORTRAN Program for Calculating Velocities and Streamlines on the Hub-Shroud Midchannel Stream Surface of an Axial-, Radial-, or Mixed-Flow Turbomachine or Annual Duct. I: User's Manual. NASA TN D-8430, 1977.
4. Katsanis, T.: FORTRAN Program for Calculating Transonic Velocities on a Blade-to-Blade Stream Surface of a Turbomachine. NASA TN D-5427, 1969.
5. McNally, W. D.: FORTRAN Program for Calculating Compressible Laminar and Turbulent Boundary Layers in Arbitrary Pressure Gradients. NASA TN D-5681, 1970.
6. Boyle, R. J.; Haas, J. E.; and Katsanis, T.: Comparison Between Measured Turbine Stage Performance and the Predicted Performance Using Quasi-3D Flow and Boundary Layer Analyses. NASA TM-83640, 1984.
7. Wood, J. R.: Improved Method for Calculating Transonic Velocities on Blade-to-Blade Stream Surfaces of a Turbomachine. NASA TP-1772, 1981.

TABLE I.—TURBINE DESIGN PARAMETERS

| Parameter	Hot engine	Standard air equivalent	Test conditions
Turbine inlet temperature, T'_1, K	1478	288.2	323
Turbine inlet pressure, P'_1, bars	9.1	1.01	1.43
Mass flow rate, m, kg/sec	0.952	0.246	0.328
Rotative speed, N, rpm	70 000	31 460	33 320
Specific work, $\Delta h'$, J/g	307.3	62.1	69.7
Torque, Γ, N-m	39.9	4.64	6.55
Power, kW	293	15	22.4
Turbine total pressure ratio, P'_1/P'_3	2.57	2.77	2.77
Total efficiency, η'	0.85	0.85	0.85
Work factor, $\Delta V_u/U_m$	1.67	1.67	1.67
Reynolds number, $m/\mu r_m$	3.12×10^5	2.35×10^5	3.12×10^5

TABLE II.—STATOR DESIGN PARAMETERS

Parameter	Hub	Mean	Tip
Profile radius at trailing edge, cm	5.331	5.857	6.383
Actual chord, c, cm	2.102	2.102	2.102
Axial chord, c_x, cm	1.607	1.607	1.607
Leading-edge radius, cm	0.152	0.152	0.152
Trailing-edge radius, cm	0.030	0.030	0.030
Trailing-edge blockage, percent	16.6	15.1	13.9
Inlet vane angle, deg	15.0	15.0	15.0
Incidence, deg	−15.0	−15.0	−15.0
Exit vane angle, deg	72.4	72.4	72.4
Solidity, c/s	1.76	1.60	1.47
Vane number		28	
Vane height at trailing edge, cm		1.052	
Aspect ratio		0.5	

TABLE III.—STATOR COORDINATES

(a) Profile coordinates

(b) Endwall coordinates
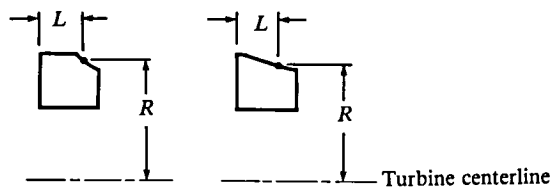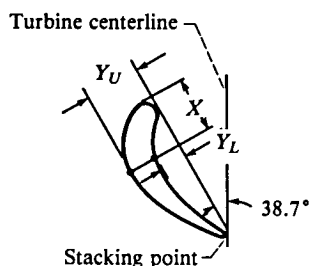
Contoured stator A Contoured stator B

X, cm	Y_L, cm	Y_U, cm
0	0.152	0.152
.102	.009	.377
.203	.009	.502
.305	.080	.590
.406	.153	.652
.508	.218	.692
.610	.274	.713
.711	.318	.719
.813	.347	.713
.914	.363	.697
1.016	.368	.673
1.118	.360	.642
1.219	.344	.604
1.321	.319	.559
1.422	.287	.509
1.524	.249	.452
1.625	.208	.390
1.727	.163	.324
1.829	.116	.253
1.930	.067	.179
2.037	.017	.101
2.103	.030	.030

L, cm	R, cm
0	6.751
1.016	6.751
1.041	6.749
1.092	6.739
1.143	6.718
1.194	6.675
1.245	6.607
1.295	6.548
1.346	6.502
1.397	6.467
1.448	6.439
1.499	6.416
1.549	6.398
1.600	6.388
1.607	6.383

L, cm	R, cm
0	6.751
.025	6.751
.076	6.749
.127	6.739
.152	6.731
.254	6.706
.508	6.642
.767	6.581
1.016	6.518
1.270	6.454
1.501	6.398
1.549	6.388
1.600	6.383
1.607	6.383

17

TABLE IV.—ROTOR DESIGN PARAMETERS

Parameter	Hub	Mean	Tip
Profile radius at trailing edge, cm	5.331	5.857	6.383
Actual chord, c, cm	2.102	2.102	2.102
Axial chord, c_x, cm	2.062	2.062	2.062
Leading-edge radius, cm	0.081	0.081	0.081
Trailing-edge radius, cm	0.036	0.036	0.036
Trailing-edge blockage, percent	12.0	10.9	10.0
Inlet blade angle, deg	40.5	40.5	40.5
Incidence, deg	16.2	7.7	−6.1
Exit blade angle, deg	−57.4	−57.4	−57.4
Solidity, c/s	1.88	1.71	1.57
Blade number		30	
Blade height at trailing edge, cm		1.052	
Aspect ratio		0.5	

TABLE V.—ROTOR COORDINATES

Turbine centerline
10.3°
X
Y_U
Y_L
Stacking point, Z
($X = 0.958$ cm, $Y = 0.467$)
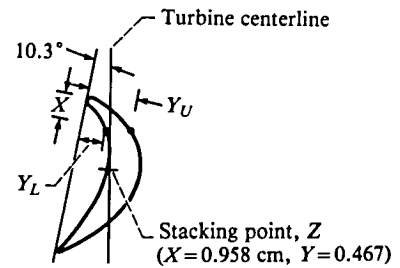
X, cm	Y_L, cm	Y_U, cm
0.102	0.082	0.082
.102	.003	.269
.203	.080	.414
.305	.165	.540
.406	.243	.645
.508	.311	.733
.610	.369	.802
.711	.415	.853
.813	.449	.888
.914	.470	.907
1.016	.478	.909
1.118	.475	.895
1.219	.459	.865
1.321	.434	.819
1.422	.398	.758
1.524	.353	.683
1.626	.300	.594
1.727	.239	.494
1.829	.171	.384
1.930	.097	.265
2.037	.018	.139
2.103	.036	.036

	Cylindrical endwall stator		Contoured stator A		Contoured stator B	
Stator kinetic energy losses ($\bar{e}_s$):						
Profile and mixing	0.029	[a](0.027)	0.027	[a](0.025)	0.026	[a](0.024)
Endwall friction	.018	(.017)	.017	(.016)	.017	(0.16)
Secondary	.011	(.010)	.009	(.010)	.012	(.011)
Incidence	.001	(.001)	.000	(.001)	.000	(.001)
Total	0.059	(0.055)	0.053	(0.052)	0.055	(0.052)
$\Delta\eta'_{stage}$	0.039		0.030		0.034	
P'_1/P_2	2.01	(2.01)	1.82	(1.82)	1.91	(1.82)
Measured stator $\bar{e}_s$		(0.055)		(0.052)		(0.052)
Rotor kinetic energy losses ($\bar{e}_R$):						
Profile and mixing	0.036		0.032		0.032	
Hub endwall friction	.008		.006		.008	
Secondary	.034		.024		.030	
Incidence	.026		.007		.013	
Tip clearance	.083		.082		.082	
Disk windage	.002		.002		.002	
Total	0.189		0.153		0.167	
$\Delta\eta'_{stage}$	0.109		0.105		0.104	
P'_2/P_3	1.85		2.05		1.93	
Exhaust duct loss, $\Delta\eta'_{stage}$	0.005		0.006		0.005	
Computed stage efficiency	0.847		0.859		0.857	
Rotor reaction, R_x	0.262		0.352		0.307	
Total pressure ratio, P'_1/P'_3	2.77		2.77		2.77	
Measured stage efficiency	0.845		0.851		0.853	

[a]Numbers in parentheses are the computed loss values using the stator inlet temperatures and pressures from ref. 2 (corresponding to a Reynolds number of about 4.1×10^5).

TABLE VII.—COMPARISON OF COMPUTED LOSSES WITH CONSTANT STATOR PRESSURE RATIO

	Cylindrical endwall stator	Contoured stator A	Contoured stator B
Stator kinetic energy losses ($\bar{e}_s$):			
Profile and mixing	0.029	0.023	0.024
Endwall friction	.018	.017	0.17
Secondary	.011	.010	.011
Incidence	.001	.001	.001
Total	0.059	0.051	0.053
$\Delta\eta'_{stage}$	0.039	0.034	0.35
P'_1/P_2	2.01	2.01	2.01
Rotor kinetic energy losses ($\bar{e}_R$):			
Profile and mixing	0.036	0.033	0.034
Hub endwall friction	.008	.008	.009
Secondary	.034	.030	.032
Incidence	.026	.025	.024
Tip clearance	.083	.087	.086
Disk windage	.002	.002	.002
Total	0.189	0.185	0.187
$\Delta\eta'_{stage}$	0.109	0.107	0.107
P^*_2/P_3	1.85	1.84	1.84
Exhaust duct loss, $\Delta\eta'_{stage}$	0.005	0.004	0.005
Computed stage efficiency	0.847	0.855	0.853
Rotor reaction, R_x	0.262	0.263	0.262
Total pressure ratio, P'_1/P^*_3	2.77	2.77	2.77

1. Report No. NASA TP-2309 AVSCOM TR 84-C-5	2. Government Accession No.	3. Recipient's Catalog No.
4. Title and Subtitle Analytical and Experimental Investigation of Stator Endwall Contouring in a Small Axial-Flow Turbine II - Stage Results .		5. Report Date September 1984
		6. Performing Organization Code 535-05-12
7. Author(s) Jeffrey E. Haas and Robert J. Boyle		8. Performing Organization Report No. E-2050
		10. Work Unit No.
9. Performing Organization Name and Address NASA Lewis Research Center and Propulsion Laboratory U.S. Army Research and Technology Laboratories (AVSCOM) Cleveland, Ohio 44135		11. Contract or Grant No.
		13. Type of Report and Period Covered Technical Paper
12. Sponsoring Agency Name and Address National Aeronautics and Space Administration Washington, D.C. 20546 and U.S. Army Aviation Systems Command, St. Louis, Mo. 63120		14. Sponsoring Agency Code

15. Supplementary Notes

Jeffrey E. Haas, Propulsion Laboratory, U.S. Army Research and Technology Laboratories (AVSCOM); Robert J. Boyle, Lewis Research Center.

16. Abstract

An experimental and analytical investigation was conducted to determine the effect of stator endwall contouring on turbine stage performance. In this investigation three stator configurations were evaluated using a common rotor. The three stator configurations were a cylindrical endwall design and two contoured endwall designs, one having a S-shaped outer wall profile and the other having a conical-shaped outer wall profile. Experimental data were obtained over a range of equivalent speeds, total pressure ratios, and rotor tip clearances for each stator-rotor combination. Detailed analytical loss assessments were conducted to aid in the determination of the contouring effect on turbine performance.

17. Key Words (Suggested by Author(s)) Axial flow turbine Endwall contouring Stator contouring Loss analysis	18. Distribution Statement Unclassified - unlimited STAR category 07		
19. Security Classif. (of this report) Unclassified	20. Security Classif. (of this page) Unclassified	21. No. of pages 23	22. Price* A02